

VOLUMETRIC VASCULAR BAIN IMAGING IN SMALL ANIMALS WITH NEAR-INFRARED OPTICAL TOMOGRAPHY

A. Y. Bluestone^{a,b}, M. Stewart^a, J. Lasker^a, G. Abdoulaev^a, A. H. Hielscher^{a,b}

a) Depts. of Biomedical Engineering and Radiology, Columbia University,
500 West 120th Street, MC 8904, New York, NY 10027.

b) Dept. of Pathology and Program in Neural and Behavioral Science,
State University of New York - Downstate Medical Center, 450 Clarkson Avenue, Brooklyn, NY 11203.

ABSTRACT

We performed three-dimensional optical tomographic brain imaging studies on small animals. Using near-infrared continuous light to probe rat brains, we were able to test our diffuse optical tomographic reconstruction algorithm. The preliminary experimental results focused on visualizing the hemodynamics in the rat head in response to perturbations in the inspired CO₂ concentration. Good agreement with observed and known physiological phenomena was obtained.

1. INTRODUCTION

Noninvasive examination of the hemodynamics of brain tissue in-vivo is of general interest in many areas of medicine and physiology. For example, some researchers are interested in studying the combined effects of low arterial blood oxygenation and abnormal cerebral blood flow in the brain [1]. Others try to obtaining realistic maps of the neuronal populations that become active during particular functional tasks [2]. Optical tomographic imaging (OTI) has emerged in recent years as a non-invasive technique that enables one to display maps of concentration changes in oxygenated and deoxygenated hemoglobin [3,4,5]. These noninvasive optical monitoring systems detect changes in optical attenuation caused by intrinsic chromophores, the most important of which is hemoglobin, and hence are capable of monitoring the hemodynamic state. Also, near-infrared optical measurements can be taken repeatedly and rapidly which allows for the dynamic study of the brain.

Most optical tomographic brain studies to date report on topographic maps, where signals obtained from within the brain are projected onto two-dimensional surface maps. These studies have convincingly demonstrated that motor-task-provoked and visual-task-provoked vascular changes can be monitored with optical techniques. However, using topographic maps it is difficult to accurately localize the source of a given signal in three-dimensional space.

Recently, our group has presented the first three-dimensional, volumetric reconstruction of hemodynamics changes occurring in the human head during a Valsalva maneuver [6]. While the results can be explained in terms of the underlying physiology, the arguments are not conclusive. What is needed is a means of reliably quantifying the spatial distribution of the observed changes. For this reason we now focus on small-animal studies, in which well-controlled protocols allow for more accurate validating of our 3-dimensional image reconstructions codes. Furthermore, small animal models are well suited for studying the neurovascular coupling in the brain. In this work we present some preliminary experimental results, which illustrate the potential of near-infrared optical tomographic imaging systems for small-animal brain imaging.

2. METHODS

2.1. Data acquisition

For the current study, we employed a continuous wave measurement system recently developed by Schmitz *et al* [7,8,9]. Light produced by laser diodes operating at wavelengths of 777 nm and 807 nm is intensity modulated at 5 KHz and 7 KHz, respectively, and optically coupled into transmitting fibers so as to provide simultaneous dual-wavelength illumination at each source site. This dual-wavelength configuration allowed for the discrimination between variations in oxyhemoglobin and deoxyhemoglobin [6,7]. Tomographic measurements, involving 4 sources and 12 detectors resulting in 48 source-detector pair were performed at a frame rate of ~ 3 Hz throughout the acquisition period, which lasted approximately two minutes.

2.2. Reconstruction

To obtain volumetric images of changes in blood parameters inside the brain we used a model-based iterative image reconstruction (MOBIIR) scheme recently developed in our group.[6] This code uses the diffusion equation as a model for light propagation in tissue. Using

a finite-element discretization the diffusion equation is solved to provide predictions of the measurement values on the boundary of the head, given a guess of optical properties inside the head. This guess is updated by employing an adjoint differentiation scheme.

In order to apply our MOBIIR scheme to the acquired data a geometric model of the underlying tissue must be generated and exact knowledge of the source detector locations must be provided. To model the geometry the anatomical volume beneath the imaging probe was modeled as a rectangular parallelepiped and converted into a three-dimensional mesh that could be used within the context of our finite-element reconstruction algorithm. The resulting volume was $12 \times 7 \times 10 \text{ mm}^3$ cube composed of 2830 nodes and 13,728 tetrahedral elements. To determine the exact source detector locations the imaging probe consisted of a fixed 4×4 array with sources, positioned at the each of the 4 corners, and detectors at the remaining sites. All optodes were separated by 1.5 mm from their nearest neighbors. A sketch of the probe is displayed in Fig. 1.

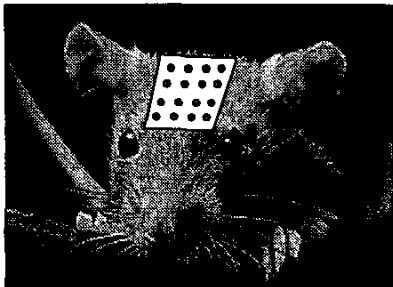


Fig. 1: Geometry of the 4 sources (red) and 12 detectors (blue) rat-imaging probe superimposed over the surface of the rat's forehead.

2.3. Animal Model and Measurement Protocol

Three-month-old Wistar rats were initially anesthetized with Halothane. Then 0.25cc of pentobarbital was administered *i.p.* as maintenance anesthetic. A tracheotomy was performed and the rat was respirated at a rate of 15 breaths per minute and a stroke volume of 15cc. The rat was then transferred to a stereotactic frame. The skin overlying the cortex was shaved and the optical probe was positioned between the anterior and posterior suture lines; bregma and lambda, respectively. For the duration of the experiment blood pressure, heart rate, and peripheral SO_2 was measured using a femoral blood pressure transducer and pulse oximeter, respectively. For the experimental protocol a baseline measurement was recorded and then the respirated CO_2 content was increased using a dual gas flow meter while the O_2 concentration was held fixed.

The raw experimental measurement data consisted of a time series for each source and each wavelength that

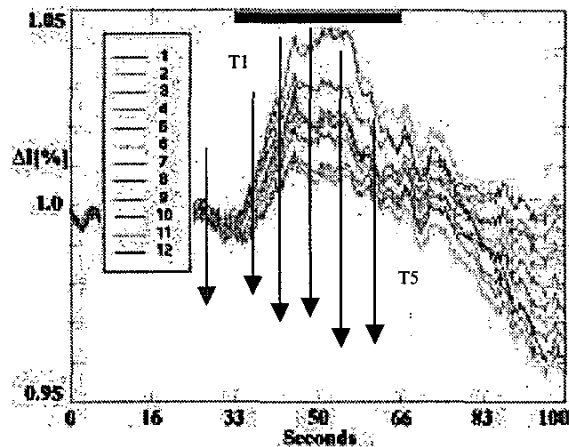


Fig.2a: Intensity change (normalized to rest at $t = 0$) as a function of time for source 2 and all 12 detectors at a wavelength of $\lambda = 777 \text{ nm}$.

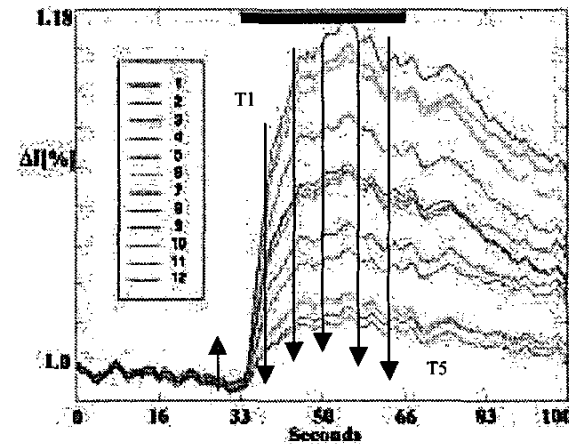


Fig.2b: Intensity change (normalized to rest at $t = 0$) as a function of time for source 2 and all 12 detectors at a wavelength of $\lambda = 808 \text{ nm}$.

depicted the change in signal strength as a function of time, as can be seen in Fig. 2. Five representative time points were selected and each data set was supplied as input to our three-dimensional MOBIIR algorithm that has been described in detail elsewhere. This procedure allows for the simultaneous reconstruction of both μ_a and D within our domain of interest from an initial guess of the optical properties. The image reconstruction process was started with an initial guess of optical properties ($\mu_a = 0.1 \text{ cm}^{-1}$, $D = (3(\mu_a + \mu_s))^{-1} = 0.042 \text{ cm}$). It should be noted that some degree of cross talk between the μ_a and D reconstructions could occur. Hence, some of the oxyhemoglobin and deoxyhemoglobin effects may be attributed to scatter changes.

3. RESULTS

3.1. CO₂-perturbation

Traces of the measured output produced by the DYNOT system at $\lambda = 777$ nm and 807 nm during the CO₂ perturbation are shown in Fig. 2. This figure displays 12 traces of detector readings during the protocol with a source at position number 2 (upper right in Fig.1). Each trace was normalized by calculating the mean of the measured intensity during the steady-state period, and subsequently dividing all intensities in the trace by that mean. Furthermore, the original data was filtered to enhance the signal to noise ratio, by using the median filter which produced a smooth function without much distortion in the overall intensity profile. The black bar in the figure depicts the extent of the CO₂ perturbation, and the arrows are the time points used for the reconstruction. At 777 nm one can observe an initial increase in intensity followed by a plateau that is present during the remainder of the perturbation. At 807 nm, an increase in intensity is observed during the first 10 seconds, followed by a drop in intensity that continues even after the provocation has ceased.

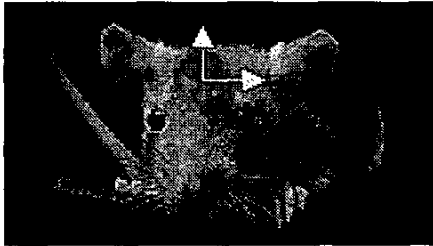


Fig. 3: Approximate location of the isosurfaces in relation to the source detector array. The coronal sections are taken in the plane defined by the arrows.

For the volumetric difference reconstructions we used the ratio of the measured intensity during a time point (black arrows labeled T₁-T₅) with respect to the measured intensity during the rest-state, red arrow (Fig. 3). These black arrows represent a snapshot (time point) of measured intensity for all source/detector combinations during consecutive instances of induced hypercapnia. For each snapshot a volumetric reconstruction of $\Delta\mu_a$ and ΔD was performed, which resulted in three volumetric images of changes in oxyhemoglobin, deoxyhemoglobin, and total hemoglobin in the rat forehead. Each reconstruction consisted of 25 iterations of the conjugate gradient scheme and took 4 hours each on a Pentium III 550 MHz processor. A representative volumetric pair of images pertaining to the peak change in deoxyhemoglobin and oxyhemoglobin is displayed in Fig. 4a, and 4b, respectively. The coronal slices in Fig. 5 were cut

midway through the isosurfaces seen in Fig. 4. Each coronal slice refers to an arrow in figure 3, T1 is the uppermost and T5 is the lowest. As one views the series from top to bottom one can observe a steady increase in deoxyhemoglobin which is circumscribed and symmetrically located.

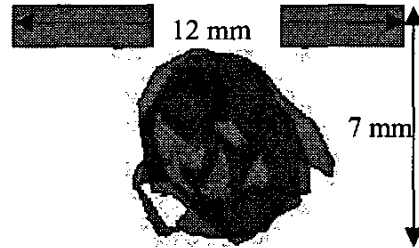


Fig. 4a: Isosurface of a 0.18mM change (increase) in deoxyhemoglobin [Hb] inside the rat head. A 2-mm layer of skin and skull is located on top of the shown image.

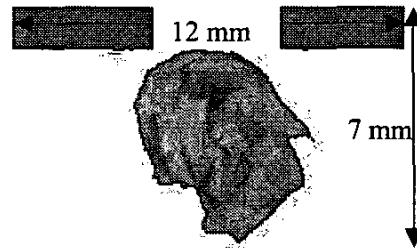


Fig. 4b: Isosurface of a 0.29mM change (decrease) in oxyhemoglobin [HbO₂] inside the rat head. A 2-mm layer of skin and skull is located on top of the shown image.

4. SUMMARY AND OUTLOOK

We have performed experiments attesting to the feasibility of using diffuse optical tomography for in-vivo small animal brain imaging. We have generated a three-dimensional mesh of the volume beneath the rat's skull and reconstructed oxyhemoglobin and deoxyhemoglobin changes in response to global respiratory provocations in carbon dioxide. The resulting data set was then used to perform 3-dimensional reconstructions and corroborate the hemodynamic changes with the known physiologic response during hypercapnia. In the future we plan to localize the hemodynamic response to a specific subsection of the brain via a syringe-induced focal hematoma. Hence a measurable and quantifiable change in hemoglobin concentration should be observed.

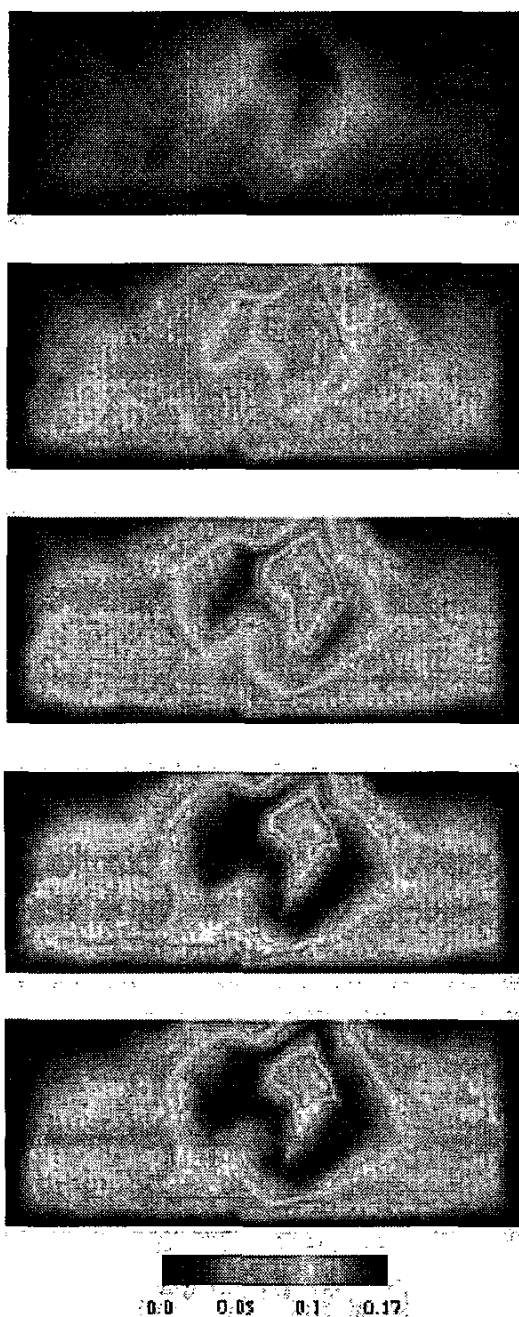


Fig. 5: Maps of deoxyhemoglobin changes for coronal sections through the plane defined by the arrows in figure 3. Concentration changes in hemoglobin are given in units of [mM]. One can see an increase in deoxyhemoglobin as one progresses from T1 (top) through T5 (bottom).

5. ACKNOWLEDGEMENTS

We would like to thank Dr. C. Schmitz and Prof. R. Barbour, State University of New York - Downstate Medical Center, Brooklyn, NY, for their assistance in setting up the near-infrared continuous-wave imaging system. This work was supported in part by the New York City Council Speaker's Fund for Biomedical Research: Toward the Science of Patient Care and an SBIR grant (2R44-HL-61057-02) from the National Heart, Lung, and Blood Institute (NHLBI) at the National Institutes of Health (NIH).

5. REFERENCES

- [1] Y. Hoshi, N. Kobayashi, M. Tamura, "Interpretation of near-infrared spectroscopy signals: a study with a newly developed perfused rat brain model," *J. Appl. Physiol.* **90**, 1657-1662 (2001).
- [2] G. Gratton, M. Fabiani, "Dynamic brain imaging: Event-related optical signal (EROS) measures of the time course and localization of cognitive-related activity", *Psychonomic Bulletin and Review* **5**, 535-563 (1995).
- [3] S. Fantini, D. Huebert, M. A. Franceschini, E. Gratton, W. Rosenfeld, P. G. Stubblefield, D. Maulik, and M. Stankovic, "Non-invasive optical monitoring of the newborn piglet brain using continuous-wave and frequency-domain spectroscopy," *Phys. Med. Biol.* **44**, 1543-1563 (1999).
- [4] M. Franceschini, V. Toronov, M. E. Filiaci, E. Gratton, S. Fantini, "On-line optical imaging of the human brain with 160-ms temporal resolution," *Optics Express* **6**, 49-57 (2000).
- [5] M. Tamura, Y. Hoshi, and F. Okada, "Localized near-infrared spectroscopy and functional optical imaging of brain activity," *Philosophical Transact. of the Royal Soc. of London - Series B: Biological Sciences.* **352**, 737-42 (1997).
- [6] A.Y. Bluestone, G. Abdoulaev, C.H. Schmitz, R.L. Barbour, A.H. Hielscher, "Three dimensional optical tomography of hemodynamics in the human head," *Optics Express* **9**, 272-287, 2001.
- [7] C.H. Schmitz, M. Löcker, J.M. Lasker, A.H. Hielscher, R.L. Barbour, "Instrumentation for fast functional optical tomography," *Review of Scientific Instrumentation*, in press.
- [8] C.H. Schmitz, Y. Pei, H.L. Graber, J.M. Lasker, A.H. Hielscher, R.L. Barbour, "Instrumentation for real-time dynamic optical tomography," in *Photon Migration, Optical Coherence Tomography, and Microscopy*, S. Andersson-Engels, M.F. Kaschke, eds., SPIE-The International Society for Optical Engineering, Proc. 4431, pp. 282-291, 2001.
- [9] C.H. Schmitz, M. Löcker, J. Lasker, A.H. Hielscher, R.L. Barbour, "Performance characteristics of a silicon-photodiode-based instrument for fast functional optical tomography," in *Optical Tomography and Spectroscopy of Tissue IV*, B. Chance, R.R. Alfano, B.J. Tromberg, M. Tamura, and E.M. Sevick-Muraca, eds., SPIE-The International Society for Optical Engineering, Proc. 4250, pp. 171-179, 2001.